Analysis & Sensing

Supporting Information

Unimolecular Cucurbit[7]uril-Based Indicator Displacement Assay with Dual Signal-Readout for the Detection of Drugs

Pierre Picchetti,* Maria Vittoria Balli, Seth Baker, Nilima Manoj Kumar, Patrick Gruhs, Luca Prodi, and Frank Biedermann*

Supporting Information

Unimolecular Cucurbit[7]uril-Based Indicator Displacement Assay with Dual Signal-Readout for the Detection of Drugs

Pierre Picchetti,*[a] Maria Vittoria Balli,[b] Seth Baker,[c] Nilima Manoj Kumar,[a] Patrick Gruhs,[a] Luca Prodi,[b] Frank Biedermann,*[a]

[a]Karlsruhe Institute of Technology (KIT), Institute of Nanotechnology (INT), Kaiserstraße 12, 76131 Karlsruhe, Germany
[b]Department of Chemistry "Giacomo Ciamician", Università degli Studi di Bologna, Via Selmi 2, Bologna, 40126, Italy
[c]Department of Chemistry, University of Victoria, 3800 Finnerty Rd., Victoria, BC V8P 5C2 (Canada) and Centre for Advanced Materials and Related Technology (CAMTEC), University of Victoria, 3800 Finnerty Rd., Victoria, BC V8W 2Y2, Canada

E-mail: pierre.picchetti@kit.edu; frank.biedermann@kit.edu

Table of Contents

1. Abbreviations

BC	Berberine chloride
CB7	Cucurbit[7]uril
CB7-NBD	Cucurbit[7]uril-4-chloro-7-nitrobenzofurazan-based chemosensor
CRE	Creatinine
CV	Cyclic voltammetry
DPV	Differential pulse voltammetry
drIDA	Dual-readout indicator displacement assay
E_{ox}	Oxidation potential
I_{em}	Emission intensity
INS	Insulin
i_{ox}	Oxidation current
j_{ox}	Oxidation current density
K_a	Binding constant
LOD	Limit of detection
NIC	(−)-Nicotine
NR	Neutral red
PB	Pancuronium bromide
PBS	Phosphate-buffered saline
PHE	L-Phenylalanine
TMA	N,N,N-trimethyl-1-damantylammonium hydroxide
SPEs	Screen-printed electrodes
UV	Ultra-Violette
VB	Vecuronium bromide
Vis	Visible
ε	Molar absorption coefficient
λ_{em}	Emission wavelength
λ_{ex}	Excitation wavelength
σ	Standard deviation
χ	Mole fraction

2. Instruments

Differential pulse voltammetry

Spectra were recorded using a Metrohm portable bipotentiostat/galvanostat (SpectroECL; ± 4 V potential range, ± 40 mA maximum measurable current). The electrochemical setup is controlled by DropView SPELEC software. For each measurement a new screen-printed carbon electrode (SPEs; DRP-110 from Metrohm DropSense; working electrode: carbon; counter electrode: carbon; pseudo-reference electrode: silver) was used for the measurements. The area of the working electrode is 0.125 cm^2. Each measurement was performed using a new SPE. For the detection of TMA and PB, changes in the j_{ox} were recorded at E_{ox} = 0.76 V, while for the detection of NIC the j_{ox} changes occurring at E_{ox} = 0.85 V were used.

Fluorescence spectroscopy

Fluorescence spectra and single-point measurements with various analytes were recorded on a CLARIOstarPlus microplate reader. OptiPlate-96 F (black, polystyrene, 96-well) wellplates were used for microplate reader-based measurements. A FLUOStar Omega microplate reader (BMG Labtech) was used to record the fluorescence spectra for cell-related experiments.

UV-Vis absorption spectroscopy

Absorbance spectra were measured at 25°C in Milli-Q water or PBS buffer on a JASCO V-730 double-beam UV-Vis spectrophotometer. For UV-Vis absorption experiments, PMMA cuvettes with a light path of 10 mm and dimensions of 10 × 10 mm from Brand with a spectroscopic cut-off at 220 nm were utilized. The samples were equilibrated by using a water thermostatic cell holder STR-812, while the cuvettes were equipped with a stirrer allowing rapid mixing.

3. Experimental details

General information

Water at Milli-Q purity was used for all experiments. Acetic acid (glacial), pancuronium bromide (pharmaceutical primary standard), vecuronium bromide (pharmaceutical primary standard), L-phenylalanine (≥ 98 %), creatinine (≥ 98 %) and (-)-nicotine (≥ 99 %) were purchased from Merck. N,N,N-trimethyl-1-adamantylammonium hydroxide (25 % in water) was purchased from BLDpharm. Insulin Human Recombinant was purchased from MP Biomedicals. Hydrochloric acid (37 % in water) was purchased from VWR. Neutral red (≥ 90 %) was purchased from ThermoFisher Scientific. Berberine chloride (≥ 98 %) was purchased from Alfa Aesar. Ammonium acetate (97 %) was purchased from Acros Organics.

The PBS buffer (1 X; 137 mM NaCl, 2.7 mM KCl, 10 mM Na_2HPO_4, and 1.8 mM KH_2PO_4) was prepared from Gibco PBS (10 X) tablets and Milli-Q water followed by further dilution with Milli-Q water (1 : 9) to achieve a 1X dilution. The pH of the PBS solution was adjusted to pH = 7.4 by adding diluted HCl (in Milli-Q water). The acetate buffer was prepared by dissolving ammonium acetate in water and adding acetic acid, whereas the pH was adjusted to pH = 3.3 using diluted HCl. To prepare the phosphate buffer (10 mM), corresponding amounts of dibasic sodium phosphate heptahydrate and monobasic sodium phosphate monohydrate were dissolved in Milli-Q water and the pH adjusted with diluted HCl.

CB7 was prepared by following procedures reported in the literature.[1]

Stock solutions of CB7-NBD and analytes were prepared in 1X PBS buffer (pH = 7.4) or acetic acid buffer (10 mM, pH = 3.3). The concentration of CB7-NBD was determined by UV-Vis absorption spectroscopy (see Figure S14) using its molar absorption coefficient (ε = 10880.446 $mol^{-1}cm^{-1}$) at 470 nm. The analyte solutions were prepared with a certain concentration directly by weighing.
OptiPlate 96-well plates (black, polystyrene, total well volume: 412 µL) were purchased from PerkinElmer.
Screen-printed carbon electrodes (model: DRP-110) were purchased from Metrohm DropSense.

Fluorescence-based detection using the drIDA

In a typical procedure, a solution of CB7-NBD (in 1X PBS buffer, pH = 7.4) was transferred to a 96-well optical plate to which a solution containing the analyte (in 1x PBS, pH = 7.4) was added so that: $c_{final,CB7\text{-}NBD}$ = 25 µM; $c_{final,analyte}$ = 0 – 100 µM; $V_{final\ per\ well}$ = 200 µL), briefly mixed with the integrated shaker of the microplate reader and left under static conditions for 3 minutes. Emission spectra were recorded from 500 to 600 nm (λ_{ex} = 470 nm). The changes in emission intensity occurring at λ_{em} = 530 nm were used for detection purposes.

DPV-based detection using the drIDA

In a typical procedure, after fluorescence-based detection (see section: fluorescence-based detection with the drIDA), 50 µL of the solution present in a well of the well plate was dropcasted onto a pre-wetted SPE. The DPV measurement was then performed. The pulse step was 0.02 V, the pulse height was 0.05 V, the pulse duration was 0.1 s, and the scan rate was 0.02 $V \cdot s^{-1}$. The DPV measurements were carried out in a potential range of 0.12 to 1.2 V.

CV studies

CB7-NBA solution with or without TMA additions was dropcasted onto a pre-wetted SPE (50 µL). The CV measurement was then performed. The potential step was 0.002 V, and the scan rate was 10, 20, 50, 100 or 200 $mV \cdot s^{-1}$. The DPV measurements were carried out in a potential range of 0.12 to 1.2 V.

4. Job plot analysis

The binding stoichiometry of CB7-NBD with PB was determined by the method of continuous variations (Job plot analysis), in which the total concentration is held constant (25 µM), while the molar fractions of CB7-NBD and PB are varied. In the reported Job's plot (Fig. S7), the I_{em} of CB7-NBD (λ_{em} = 530 nm) was recorded upon excitation λ_{ex} = 470 nm in PBS (1X, pH = 7.4). The binding stoichiometry between CB7-NBD and PB was calculated to be 1:1 (see below).

c_{total} = 25 µM, molar fraction varied from 0 to 1

$$\chi(CB7\text{-}NBD) = \frac{[CB7\text{-}NBD]}{[CB7\text{-}NBD] + [PB]}$$

Range χ = 0 – 0.5: y = 949.022 x + 5.498

Range χ = 0.5 – 1: y = 664.941 x + 147.002

Intersection: χ = 0.4981 ≈ 0.5

5. Determination of the LOD

The linear range of the calibration curves was fitted with a linear regression curve. The LOD was calculated from three independent measurements using the following equation:

$$LOD = \frac{3.3 \cdot (\sigma_{CB7\text{-}NBD})}{|slope|}$$

6. Interferent analysis

The signal response of CB7-NBD was calculated using the following formula, where the signal can represent either the emission intensity or the measured current densities:

$$signal^{rel}_{Fl\ or\ jox}\% = \left| \frac{\left(signal^{CB7\text{-}NBD}_{Fl\ or\ jox} - signal^{+interferent}_{Fl\ or\ jox}\right)}{signal^{CB7\text{-}NBD}_{Fl\ or\ jox}} \right| \times 100$$

7. Supporting figures

Structures of chemosensors with suboptimal electrochemical signal response for this study

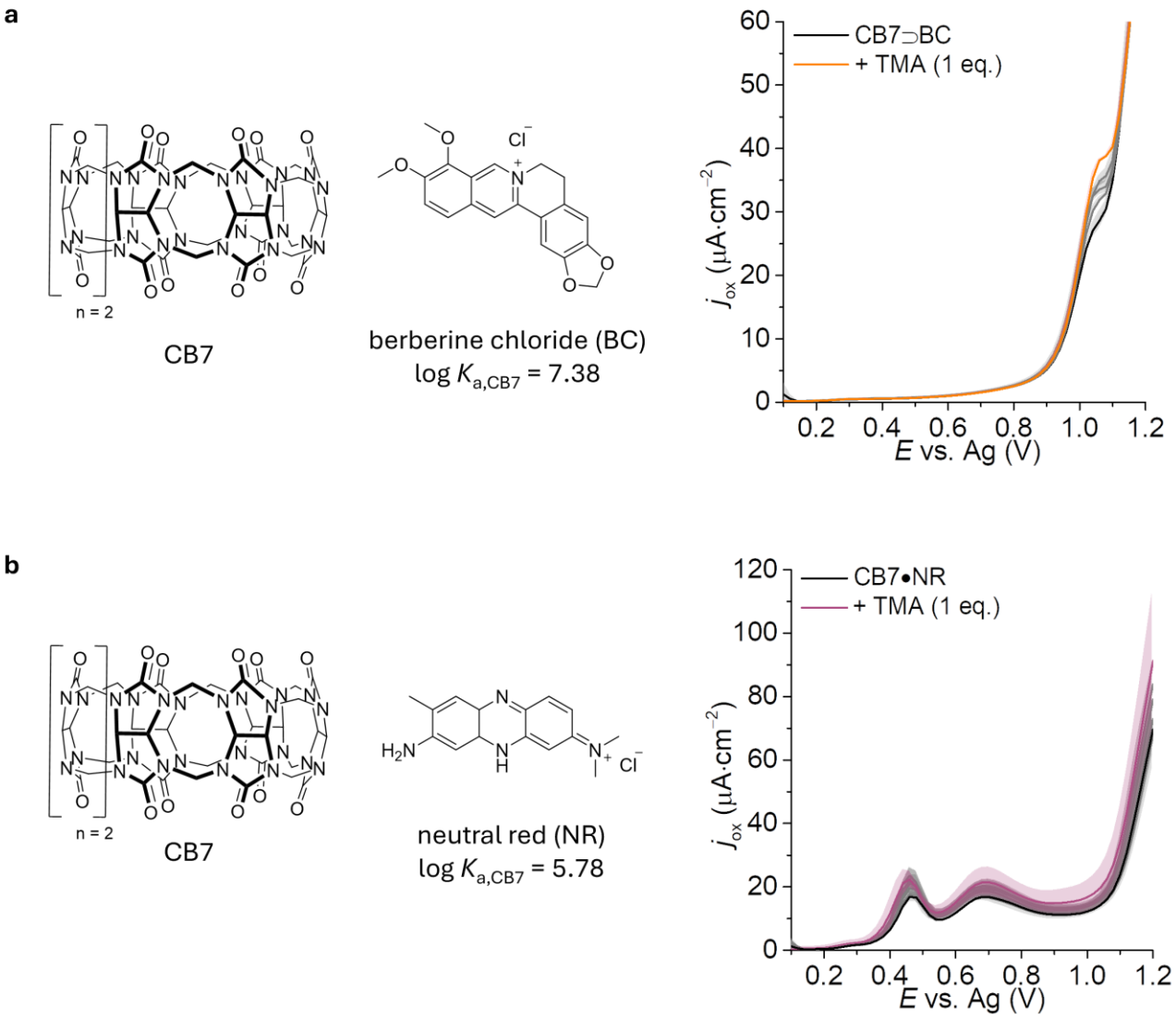

Fig. S1. (a) Chemical structures of CB7 and berberine chloride and the DPV response curves of CB7⊃BC (50 μM) in the absence and presence of TMA (0 – 50 μM). (b) Chemical structures of CB7 and neutral red and the DPV response curves of CB7-NR (50 μM) in the absence and presence of TMA (0 – 50 μM). The average intensities and corresponding standard deviations (σ) were calculated from three independent measurements. The binding constants from the literature for berberine chloride[3] and neutral red[4] are reported.

The CB7⊃BC and CB7•NR chemosensors show overlapping errors in the detection of TMA, which renders both chemosensors suboptimal for setting up an electrochemical sensor. This is likely due to molecular aggregates on the electrode surface. DPV analysis of CB7•NR showed two oxidation peaks, indicating exposed amino molecules for oxidation, even in a complex with CB7. However, the presence of TMA did not significantly alter these peaks, rendering the chemosensor ineffective for electrochemical detection.

Ion pairing effect

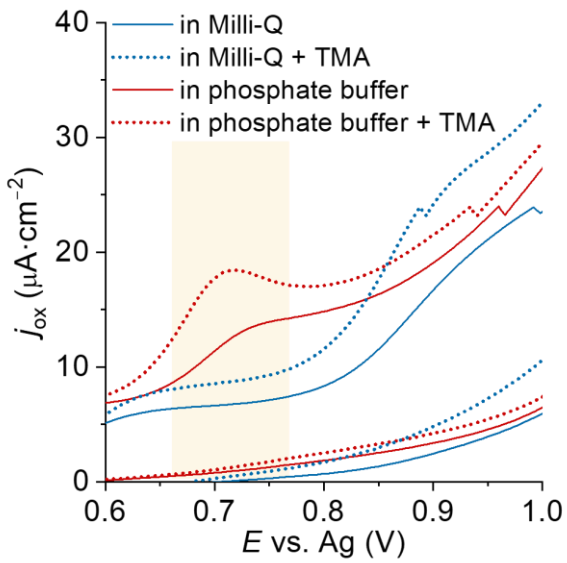

Fig. S2. Cyclic voltammetry study on the current changes occurring during the electrochemical oxidation of CB7-NBD in Milli-Q water or dissolved in phosphate buffer (10 mM, pH = 6.8). The significant increase in current at the potential at which NBD is oxidized (see yellow highlighted area) can be attributed to an ion pairing effect between the positively charged [CB7-NBD⊃TMA]$^+$ complex and the phosphate anions. In the presence of phosphate anions (at a concentration of 10 mM, as in our PBS buffer), the formation of an ion pair with the positively charged [CB7-NBD⊃TMA]$^+$ complex facilitates its migration towards the positively polarized anode. Thus, when [CB7-NBD⊃TMA]$^+$ is oxidized, ion migration strongly contributes to mass transfer to the electrode, which has a greater effect than the general change in diffusivity.

Change in DPV curves by CB7-NBD in the presence of TMA

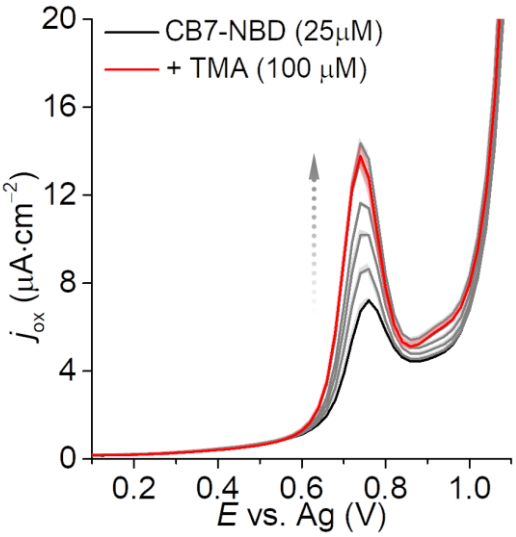

Fig. S3. DPV analysis of CB7-NBD (25 μM) in PBS (1X, pH = 7.4) without and with TMA (0 − 100 μM). The amounts of guest added were 0, 5, 10, 15, 30, 50 and 100 μM. The average intensities and corresponding standard deviations (σ) were calculated from three independent measurements.

Emission and UV-Vis absorption spectrum of CB7-NBD with and without TMA

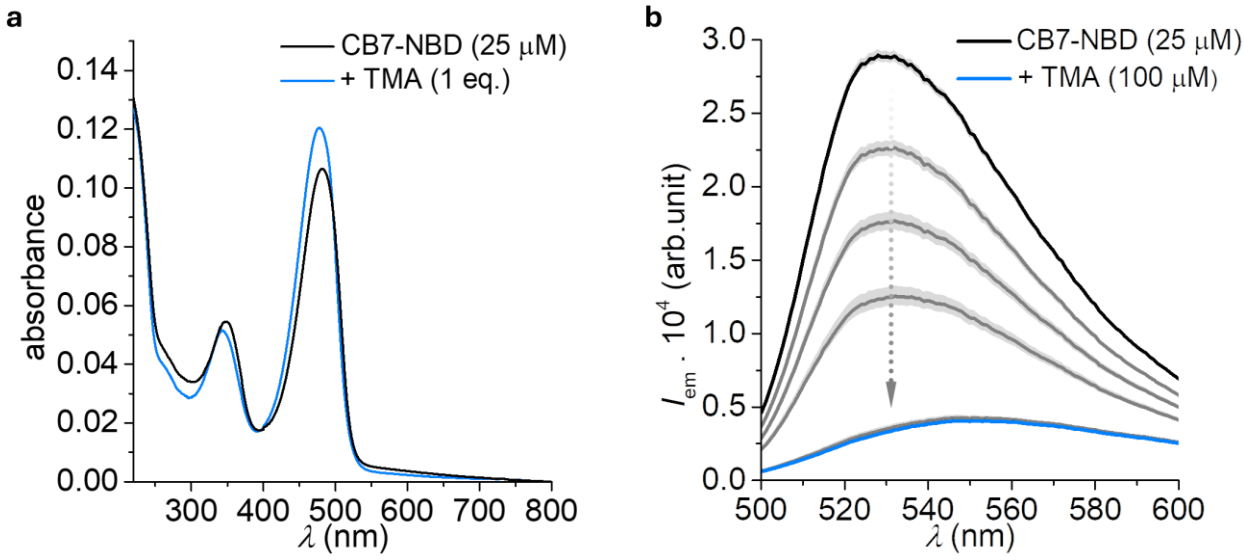

Fig. S4. (a) UV-Vis absorption spectrum of CB7-NBD (25 μM) in PBS (1X, pH = 7.4) without and with TMA (1 eq.). (b) Fluorescence spectra (λ_{ex} = 470 nm) of CB7-NBD (25 μM) with and without TMA (0, 5, 10, 15, 30 and 100 μM) of CB7-NBD (25 μM) in PBS (1X, pH = 7.4). The average intensities and corresponding standard deviations (σ) were calculated from three independent measurements.

LOD determination for the drIDA based detection of TMA

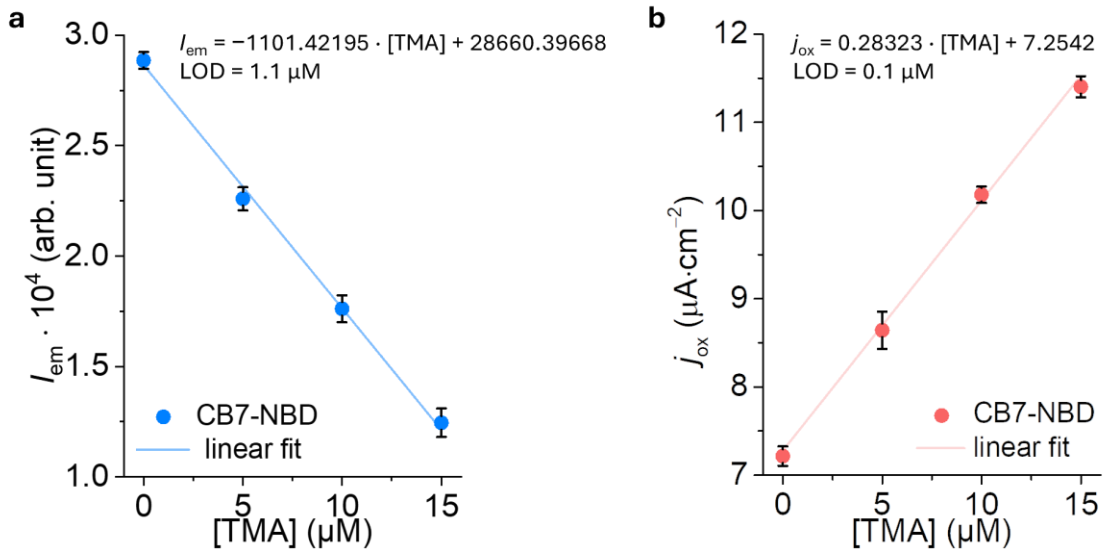

Fig. S5. Linear regime of the drIDA response curves for TMA in the (a) fluorescence and (b) DPV detection mode.

Change in fluorescence spectra and DPV curves by CB7-NBD in the presence of PB

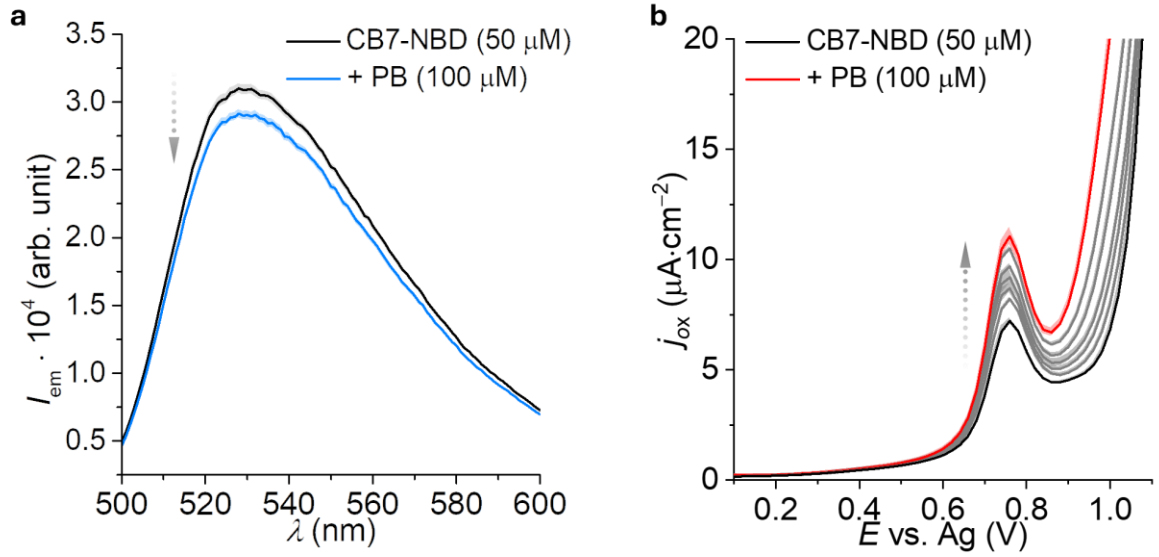

Fig. S6. (a) Fluorescence spectra (λ_{ex} = 470 nm) and (b) DPV analysis of CB7-NBD (50 µM) in PBS (1X, pH = 7.4) without and with PB (0 – 100 µM). For the DPV measurements, 0, 5, 10, 15, 30, 50 and 100 µM of the guest were added. The average intensities and corresponding standard deviations (σ) were calculated from three independent measurements.

Job plot analysis of CB7-NBD and PB

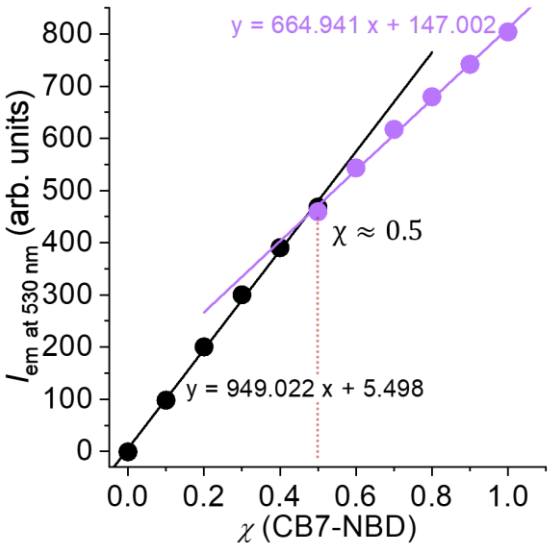

Fig. S7. Job plot analysis for determining the binding stoichiometry between CB7-NBD and PB in PBS (1X, pH = 7.4). The total concentration is held constant (25 μM), while the molar fractions of CB7-NBD and PB are varied. The emission was recorded at λ_{ex} = 470 nm.

DPV-curves for CB7-NBD and NIC at different pH

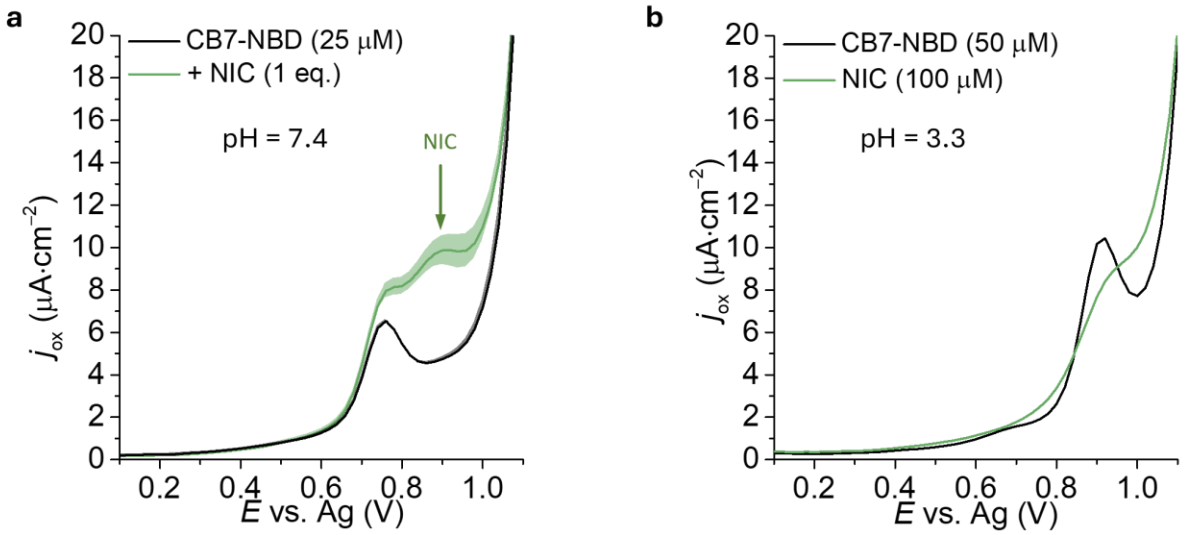

Fig. S8. (a) DPV analysis with CB7-NBD (25 μM) before and after the addition of 1 eq. of NIC. The presence of the highlighted oxidation peak at E_{ox} = 0.9 V corresponds to NIC contributing to a background signal that masks the occurrence of displacement and electrochemical oxidation of NBD. The average j_{ox} with the corresponding standard deviation were calculated from three independent measurements. (b) DPV analysis of CB7-NBD (25 μM) and NIC alone (100 μM) at pH = 3.3 (in 0.1 M acetate buffer). The acidic pH suppresses the large background signal of NIC that occurs at near neutral pH.

Change in fluorescence spectra and DPV curves by CB7-NBD in the presence of NIC

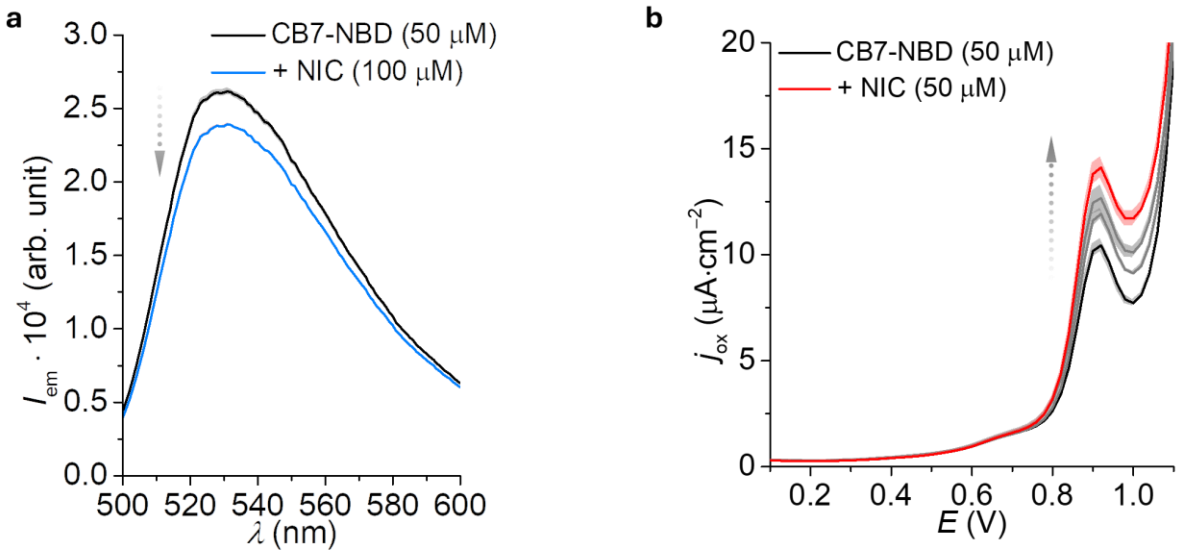

Fig. S9. (a) Fluorescence spectra (λ_{ex} = 470 nm) and (b) DPV analysis of CB7-NBD (50 μM) in acetate buffer (0.1 M, pH = 3.3) in the presence of NIC (0, 12.5, 25, 50 μM in DPV analysis). The average intensities and corresponding standard deviations (σ) were calculated from three independent measurements.

UV-Vis absorption and emission spectra of CB7-NBD at different pH values

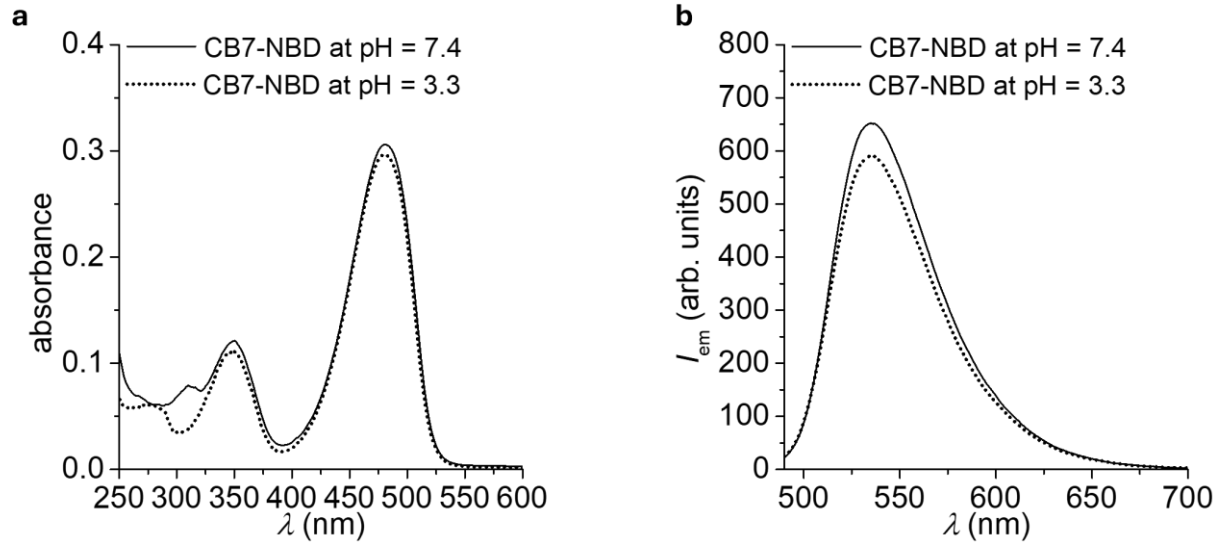

Fig. S10. (a) Absorption spectra of CB7-NBD (25μM) in in PBS (1X, pH = 7.4) or acetate buffer (0.1 M, pH = 3.3). (b) Emission spectra of CB7-NBD (25μM, λ_{ex} = 470 nm) in PBS (1X, pH = 7.4) or acetate buffer (0.1 M, pH = 3.3).

UV-Vis absorption spectra of analytes

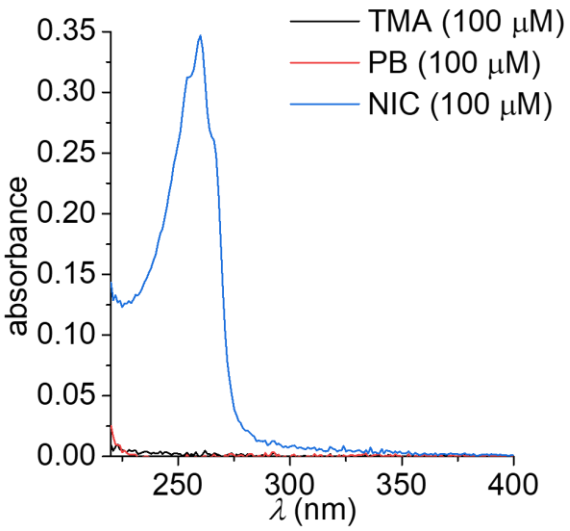

Fig. S11. UV-Vis absorption spectra of analytes in PBS (1X, pH = 7.4).

Fluorescence- and DPV-based study of potential interferences

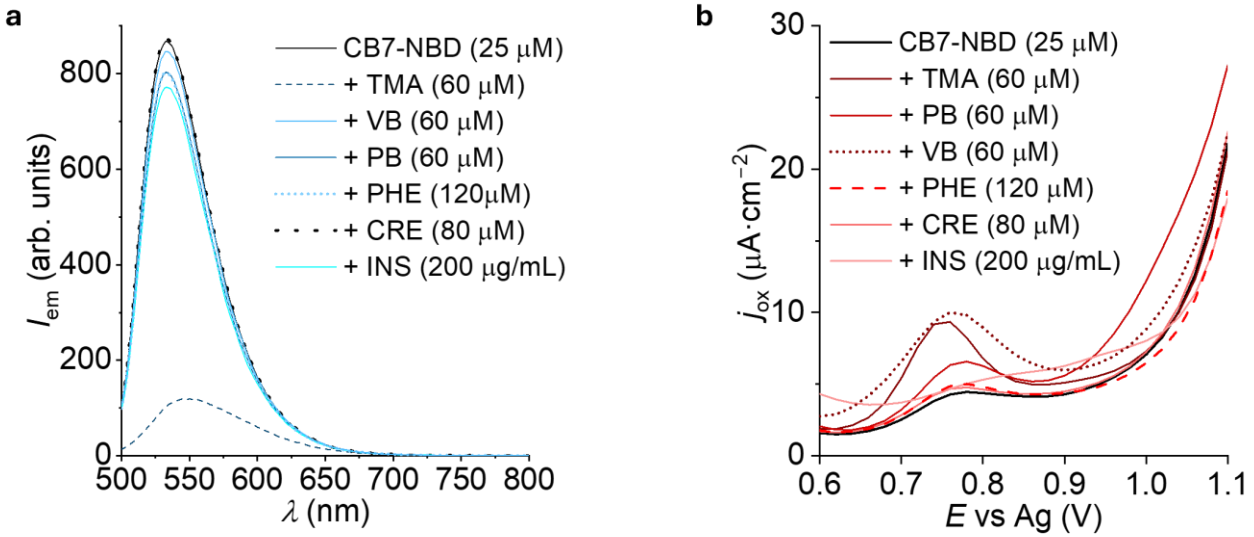

Fig. S12. (a) Fluorescence spectra (λ_{ex} = 470 nm) and (b) DPV analysis of CB7-NBD (25 μM) in PBS (1X, pH = 7.4) with interferents.

TMA detection in 7 Up

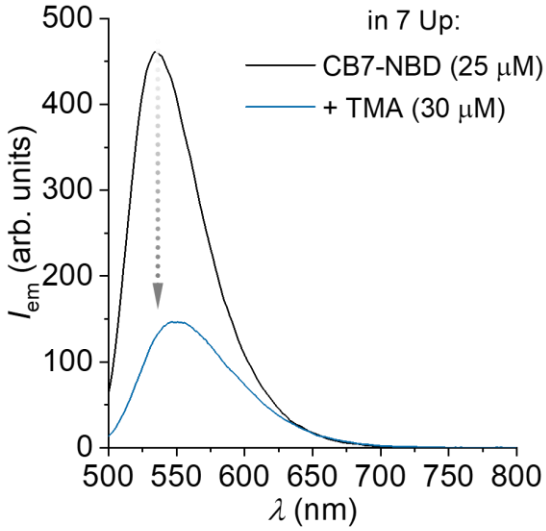

Fig. S13. Fluorescence spectra (λ_{ex} = 470 nm) CB7-NBD (25 μM) in non-diluted 7 UP soft drink without and with TMA (30 μM). 7 Up is composed of filtered carbonated water, sugar, citric acid, lemon extract, lime extract, stevia leaf extract.

Determination of the molar extinction coefficient for CB7-NBD

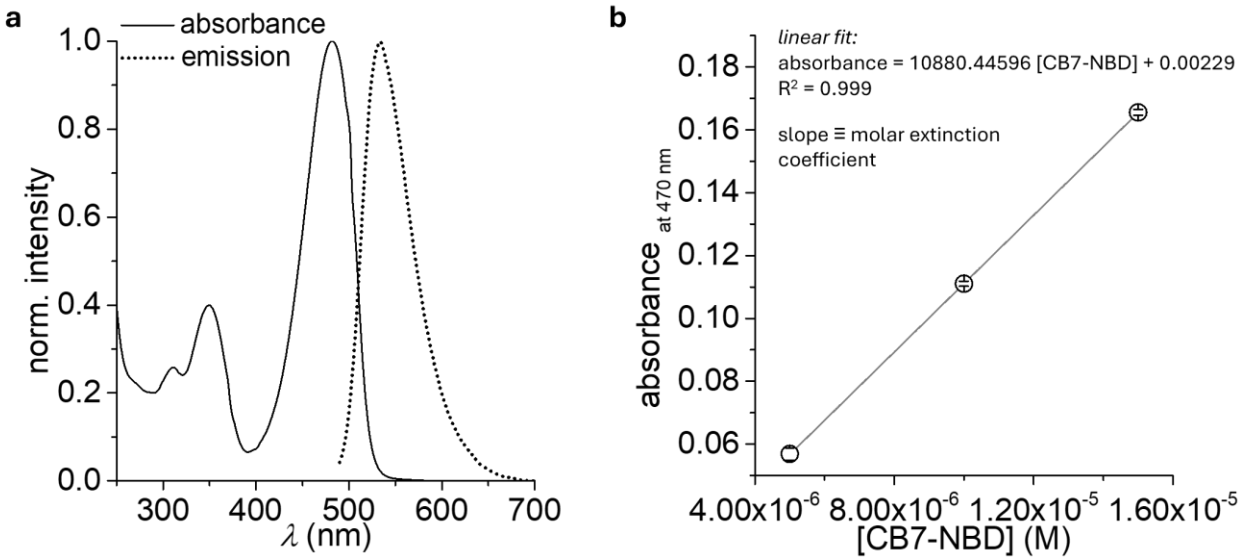

Fig. S14. (a) Normalized absorption and emission spectra (λ_{ex} = 470 nm) of CB7-NBD in PBS (1X, pH = 7.4). (b) Concentration-dependent absorption intensities for CB7-NBD at 470 nm, which were used for the calculation of $\varepsilon_{CB7\text{-}NBD}$.

8. Supporting Tables

Table S1. Calibration functions

analyte	fl. calibration function	DPV calibration function
TMA	$I_{em} = -1101.42195 \cdot [TMA] + 28660.39668$	$j_{ox} = 0.28323 \cdot [TMA] + 7.2542$
PB	$I_{em} = -40.20449 \cdot [PB] + 30932.72225$	$j_{ox} = 0.10204 \cdot [PB] + 4.85868$
NIC	$I_{em} = -45.9669 \cdot [NIC] + 25900.33089$	$j_{ox} = 0.07304 \cdot [NIC] + 10.4195$

9. References

[1] C. Marquez, F. Huang, W. M. Nau, *IEEE Trans. Nanobioscience* **2004**, *3*, 39-45.

[2] C. Hu, T. Jochmann, P. Chakraborty, M. Neumaier, P. A. Levkin, M. M. Kappes, F. Biedermann, *J. Am. Chem. Soc.* **2022**, *144*, 13084-13095.

[3] A. Prabodh, S. Sinn, L. Grimm, Z. Miskolczy, M. Megyesi, L. Biczok, S. Brase, F. Biedermann, *Chem. Commun.* **2020**, *56*, 12327-12330.

[4] J. Mohanty, A. C. Bhasikuttan, W. M. Nau, H. Pal, *J. Phys. Chem. B* **2006**, *110*, 5132-5138.